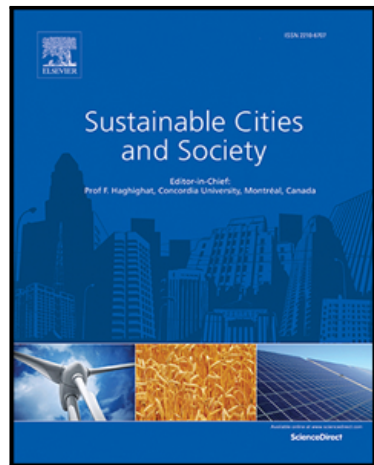


Intense drought and vegetation browning exacerbate air temperature rise in unirrigated peri-urban areas under global warming

Guillermo A. Moncada-Morales , Stephen J. Livesley ,
Kerry A. Nice , Andrea Pianella , Manuel Carpio

PII: S2210-6707(25)00517-7
DOI: <https://doi.org/10.1016/j.scs.2025.106643>
Reference: SCS 106643



To appear in: *Sustainable Cities and Society*

Received date: 14 March 2025
Revised date: 20 May 2025
Accepted date: 13 July 2025

Please cite this article as: Guillermo A. Moncada-Morales , Stephen J. Livesley , Kerry A. Nice , Andrea Pianella , Manuel Carpio , Intense drought and vegetation browning exacerbate air temperature rise in unirrigated peri-urban areas under global warming, *Sustainable Cities and Society* (2025), doi: <https://doi.org/10.1016/j.scs.2025.106643>

This is a PDF file of an article that has undergone enhancements after acceptance, such as the addition of a cover page and metadata, and formatting for readability, but it is not yet the definitive version of record. This version will undergo additional copyediting, typesetting and review before it is published in its final form, but we are providing this version to give early visibility of the article. Please note that, during the production process, errors may be discovered which could affect the content, and all legal disclaimers that apply to the journal pertain.

© 2025 Published by Elsevier Ltd.

Highlights

- Peri-urban areas in Santiago warm faster than urban parks and residential areas.
- Of the three areas, the peri-urban area has shown the greatest decreases in rainfall.
- Urban park area exhibited the largest increase in daily temperature range.
- Intra-annual variability is greater in cooler than in warmer months in peri-urban area.
- Soil drying in peri-urban areas causes the highest warming due to permeable surfaces.

Intense drought and vegetation browning exacerbate air temperature rise in unirrigated peri-urban
areas under global warming

Guillermo A. Moncada-Morales^a, Stephen J. Livesley^b, Kerry A. Nice^c, Andrea Pianella^d, Manuel Carpio^{f, a, e *}

^a Department of Construction Engineering and Management, School of Engineering, Pontificia Universidad Católica de Chile, Avenida Vicuña Mackenna 4860, Santiago, Chile

^b School of Agriculture, Food and Ecosystem Sciences, Burnley Campus, The University of Melbourne, 500 Yarra Boulevard, Richmond, Melbourne, Victoria 3121, Australia

^c Transport, Health and Urban Systems Research Lab, Faculty of Architecture, Building and Planning, The University of Melbourne, Melbourne, Australia

^d Faculty of Architecture, Building and Planning, The University of Melbourne, Victoria 3010, Australia

^e Centro Nacional de Excelencia para la Industria de la Madera (CENAMAD), Pontificia Universidad Católica de Chile, Santiago, Chile

^f Department of Construction Engineering and Project Management, University of Granada, Spain

*Corresponding author: carpio@ugr.es

Acknowledgements

This work was funded by: ANID/Scholarship Program/DOCTORATE SCHOLARSHIPS CHILE/21230600; ANID BASAL FB210015 CENAMAD; ANID FONDECYT 1201052; BG23/00134; and Pontificia Universidad Católica de Chile through the 2024 International Sabbatical Support Competition of the Academic Vice-Rectorship. The first author gratefully acknowledges the University of Melbourne for its generous support and academic mentorship during his tenure as an international research student.

ABSTRACT

Cities are particularly vulnerable to climate change, which continues to drive rising air temperatures. The morphology of a city also influences local climate through diverse surface properties and configurations, leading to diverse responses to warming trends. We examined the impact of climate change on Santiago, Chile, a valley city with a semi-arid climate. Near-surface air temperature and rainfall data from Chile's Bureau of Meteorology over the past 63 years were collected from three different local climate zones (LCZs) in a peri-urban, urban park, and residential areas. The research employed regression analysis, a seasonal time series model, and standardised anomalies to assess air temperature and rainfall trends. Results show that the peri-urban area has experienced the highest rate of warming and the greatest decline in rainfall, alongside a doubling of the warming rate in recent years. Discrepancies in maximum and minimum temperature trends resulted in varying daily temperature ranges (DTR) across LCZs. The peri-urban area also displayed significant intra-annual variability in air temperature and rainfall, leading to trend variations over the years in contrast to the other LCZs. Our findings underscore the accentuated impact of climate change in the peri-urban area due to its permeable bare soil surfaces with an increase of 0.36°C per decade of warming, compared to the areas characterised by impermeable surfaces and well-irrigated green spaces of 0.25°C per decade on average. It highlights the importance of analysing urban air temperatures through LCZ classifications, challenging the conventional urban-rural temperature dichotomy that underpins urban heat island assessments.

Keywords

Urban climate; climate change; local climate zones; Near-surface air temperature; rainfall; semiarid; Santiago

Highlights

- Peri-urban areas in Santiago warm faster than urban parks and residential areas.
- Of the three areas, the peri-urban area has shown the greatest decreases in rainfall.
- Urban park area exhibited the largest increase in daily temperature range.
- Intra-annual variability is greater in cooler than in warmer months in peri-urban area.
- Soil drying in peri-urban areas causes the highest warming due to permeable surfaces.

1. INTRODUCTION

Urbanization is a key driver of change at local, regional and global scales (Cleugh & Grimmond, 2012). It significantly alters natural surface conditions, transforming the physical environment and affecting energy and carbon exchanges, thermal conditions, moisture fluxes, and wind circulation systems (Oke et al., 2017). Different urban design types with varying surface and atmospheric properties modifications lead to distinct urban microclimates (Hall et al., 2016; Joshi et al., 2022) that are influenced by climate change (Cleugh & Grimmond, 2012) in differing ways. Studies report rising observed temperatures in urban areas worldwide (Ajaaj et al., 2018; Pingale et al., 2014) as well as an accelerating trend in recent years (Dodman et al., 2023; Hobbie & Grimm, 2020). Therefore, although increasing urban temperatures are often attributed to large-scale climate change (Masson et al., 2020), different urban landscapes within the same city can exhibit varying long-term temperature trends. This raises a critical question: To what extent and how do temperature trends differ across various urban landscapes within a city in response to climate change?

Radiative, thermal, humidity and aerodynamic properties of the urban surface characterise its spatial heterogeneity. Surface properties produce variations in temperature response depending on the climatic conditions (Lai & Cheng, 2010), so the thermal climate of a specific urbanised area will differ significantly from that of other zones with contrasting structure and cover (Stewart, 2013). Changes in rainfall patterns, primarily driven by climate change (Ohba, 2021), affect water availability and evapotranspiration (Li et al., 2016), and global warming-induced soil drying in urban areas (Lauwaet et al., 2016) can enhance intra-urban temperature contrasts. In particular, changes in daily temperature ranges (DTR) have been linked to both increased

heterogeneity in land cover and shifts in precipitation (Irizarry-Ortiz et al., 2013; Lai & Cheng, 2010). However, findings remain inconclusive, as short-term analyses sometimes report negligible trends (Bonacci & Durin, 2023), highlighting the complexity of attributing climatic changes solely to urbanisation or global warming.

Cities in the Global South are often understudied due to climate data scarcity, sparking a vigorous debate in recent years on how to understand these urban environments (Randolph & Storper, 2023). Of particular interest are cities in arid and semi-arid climates, not only because they face dry conditions and severe challenges exacerbated by climate change (Minderlein & Menzel, 2015; Shen & Chen, 2010) but also due to the limited research available on them (Licón-Portillo et al., 2024). Semi-arid climates are characterised by extreme variability, with frequent droughts and uncommon periods of above-average rainfall (Snyder & Tartowski, 2006). The west coast of South America, extending from the equator to the Mediterranean climate regime of central Chile, is dominated by semi-arid conditions. Santiago, situated in this central region, is the Chile's primary urban centre, characterised by dry summers and a cold semi-arid climate with recurrent serious impacts from droughts (Aldunce et al., 2017; Garreaud et al., 2020; Moser et al., 2018). Santiago has experienced rising heatwave frequencies coupled with drier soils during warmer months and increasing climatic stress in recent decades (Piticar, 2018; Stolpe & Undurraga, 2016); trends expected to intensify under future climate scenarios (McPhee et al., 2014).

In terms of urban design, Santiago is a chaotic mosaic of built-up areas with mixed patterns of high-rise and mid-rise buildings and low-rise houses with green areas, all of different standards (Sarricolea et al., 2022). Due to this spatial urban heterogeneity, distinguishing the impacts of local urbanisation from those of climate change on long-term air temperature trends is

challenging, particularly when comparing areas with differing urban structures and permeable and impermeable surfaces. The combination of climate change's impact on this city and its urban heterogeneity generates uncertainty in understanding the long-term urban climatic conditions and possible future climate scenarios that the city may face.

Assessing climatic conditions in urban environments relies on climate data at both local and regional scales. Numerous studies have investigated urban-scale temperature trends associated with climate change, using long-term data expressed as annual anomalies (Ajaaj et al., 2018; Bayer-Altin et al., 2024), DTR (Irizarry-Ortiz et al., 2013), seasonal patterns (Livada et al., 2019) and shifts in extreme temperature (Arsiso et al., 2018; Pingale et al., 2014). Although year-on-year differences may be minimal and intra-annual variability is often removed, such comparisons are not always like-for-like, as they may obscure trends in intra-annual data due to shifts in seasonal fluctuations. Therefore, it is necessary to analyse the time series climatic data on both inter- and intra-annual scales.

Time series analysis provides insights into climate behaviour through statistical evaluation (Mudelsee, 2019), with advanced methods improving trend estimation and uncertainty assessment, thereby supporting climate science. Regression analysis is commonly used for trend estimation, assuming the absence of outliers or their prior removal through extreme value analysis (Mudelsee, 2014). However, while linear transformations preserve data distribution and facilitate comparisons of long-term trends, they are not strictly generalisable due to locational differences. A mathematical transformation helps remove the influence of location and spread, making datasets more comparable (Wilks, 2019), and accounting for seasonal variations (Koudahe et al., 2017; Liu et al., 2018). Standardising data into anomalies further enables

meaningful comparisons of long-term changes across locations with distinct urban characteristics. Moreover, understanding irregular variations in seasonal temperature trends is crucial to describe the nature of temporal processes (Privalsky, 2023). The seasonal time series model helps identify underlying distributions and outliers through irregularity detection (Mills, 2019).

To contextualise air temperature trends within urban environments, it is essential to consider urban surface characteristics. The local climate zone (LCZ) methodology (Stewart & Oke, 2012) provides a robust framework for this purpose. The core scientific premise of the LCZs is that similar neighbourhoods exhibit comparable local climatic effects and relatively homogeneous temperatures compared to nearby neighbourhoods, a concept validated through various temperature observation techniques (Masson et al., 2020).

This study aims to assess air temperature changes over 63 years in three LCZs in a semi-arid city to understand how climate change impacts urban landscapes differently according to surface characteristics and rainfall variability, using long-term weather station data. The study seeks to answer two research questions:

- How does the inter-annual trend of air temperature in response to climate change differ across three LCZ types, which are represented by locations of: a) sparsely developed peri-urban, b) an urban park in a dense, low-rise urban, and c) an intermediate residential area; and
- How do intra-annual trends differ in response to climate change in these three different LCZs?

These research questions are based on the hypothesis that a featureless landscape with a permeable surface, predominantly bare soil, will exhibit a stronger warming response to changes in rainfall and drought than a more open, low-rise built environment with permeable green areas in a warming world. Consequently, the peri-urban area is expected to experience a more pronounced increase in air temperature than urban park and residential areas, as evapotranspiring ground surfaces without irrigation being to behave more like impervious surfaces during prolonged drought. While all LCZs will respond to global warming, their sensitivity to drought periods associated with climate change will vary.

2. MATERIAL AND METHODS

This section provides a general geographical description of the city under study, followed by a detailed explanation of the methodology, including the long-term weather station data, the analysed LCZs, and the time series methods applied.

2.1. *Santiago's climate*

The central macroregion of Chile is predominantly characterised by a temperate climate, covering 91% of this region. Tundra climates, accounting for less than 6%, are confined to high mountain areas, while arid climates occupy just 3% of the total area (Sarricolea et al., 2017). Santiago, Chile's capital and largest metropolis, with almost 8 million inhabitants, equivalent to 42.5% of the national population (INE, 2019), lies in this zone. This city is situated in a valley bordered by the Andes Cordillera to the east and the Coastal Cordillera to the west and an elevation of approximately 520 m a.s.l. The city itself has a semi-arid climate, specifically

classified as BSk and Csa under the Köppen-Geiger system (Beck et al., 2018), with rainy winters and dry summers. Precipitation concentrates in autumn, winter, and spring, while cloudless days are primarily observed in summer.

2.2. *Methodological analysis*

Fig. 1 depicts the methodological analysis framework to analyse the climate change impact in Santiago, Chile. Initially, we chose three long-term weather stations in Santiago, operated by Chile's Bureau of Meteorology, whose temperature and rainfall data were downloaded from its database (DMC, 2024). Surrounding each station, temporal observations of satellite imagery were conducted to detect changes in land cover and classify the LCZs. The satellite imagery platforms used were Google Earth Pro (2025) and the U.S. Geological Survey (2025). Finally, a time series analysis was applied, based on regression analysis, a seasonal time series model and standardised anomalies, to determine the impact of climate change on air temperature and rainfall trends in three contrasting LCZs. Additionally, ANOVA test and Spearman rank correlation coefficient was applied to examine the consistency and correlation.

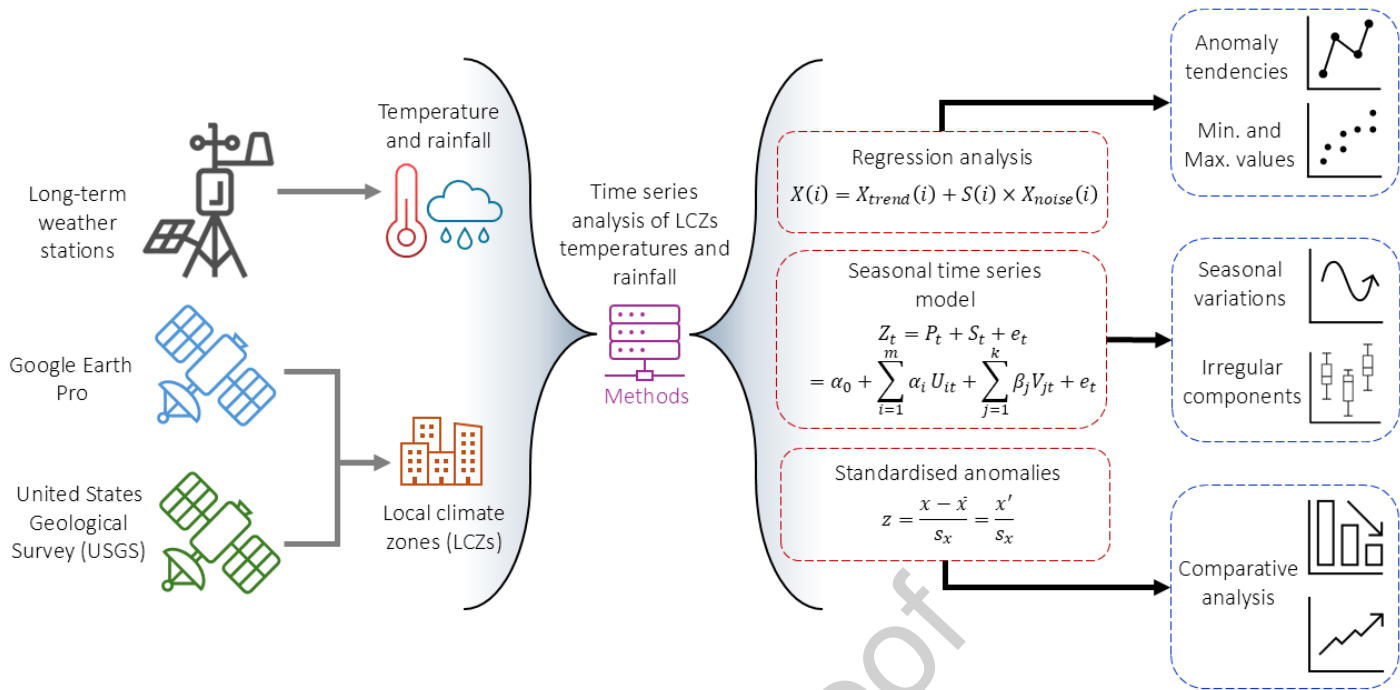


Fig. 1. Methodological analysis framework to analyse long-term temperatures of the LCZs studied. The grey arrows indicate a step process, and the black arrows reflect the products. The time series analysis is explained in section 2.6.

2.3. Weather stations and local climate zones

The three long-term weather stations in Santiago, installed since the last century, are located in the northwest, centre, and east of the city (Fig. 2). The characterisation of the location of the stations was reclassified based on the previous work of Sarricolea et al. (2022) using the LCZ methodology (Stewart & Oke, 2012). Due to deviations from standard LCZ classes, each site was assigned specific subclasses based on the surrounding built types, land cover, and geometric properties within a 500-metre radius. The notation for the subclasses is LCZ X_y , where X is the dominant class in the standard set of LCZs, and y is the lower class from the standard set. The use of these subclasses is justified as the secondary characteristics (subscript y) are expected to influence the local microclimate. This classification is particularly relevant given the study's focus on assessing the impacts of climate change in urban environments.

The first station, located in the northwest and inside the Santiago International Airport (peri-urban area), was classified as LCZ F_E, characterised by a predominance of bare soil and some paved surfaces (e.g., the aeroplane runway). The second station, in a dense, low-rise urban area, sits within an irrigated urban park with scattered trees, grass, bare ground, scattered buildings, and paved surfaces, and was classified as LCZ 9_D. However, the park is surrounded by dense, low-rise buildings with limited vegetation and covered mainly by pavements and building concrete materials. The third station, near the eastern mountains, is located at an aerodrome (Eulogio Sánchez) surrounded by compact, low-rise residential buildings. The station, positioned beside the runway, was classified as LCZ 6_D, characterised by a mix of low-rise buildings, scattered trees in irrigated gardens and streets, and pervious surfaces with minimal and no grass in the aerodrome area.

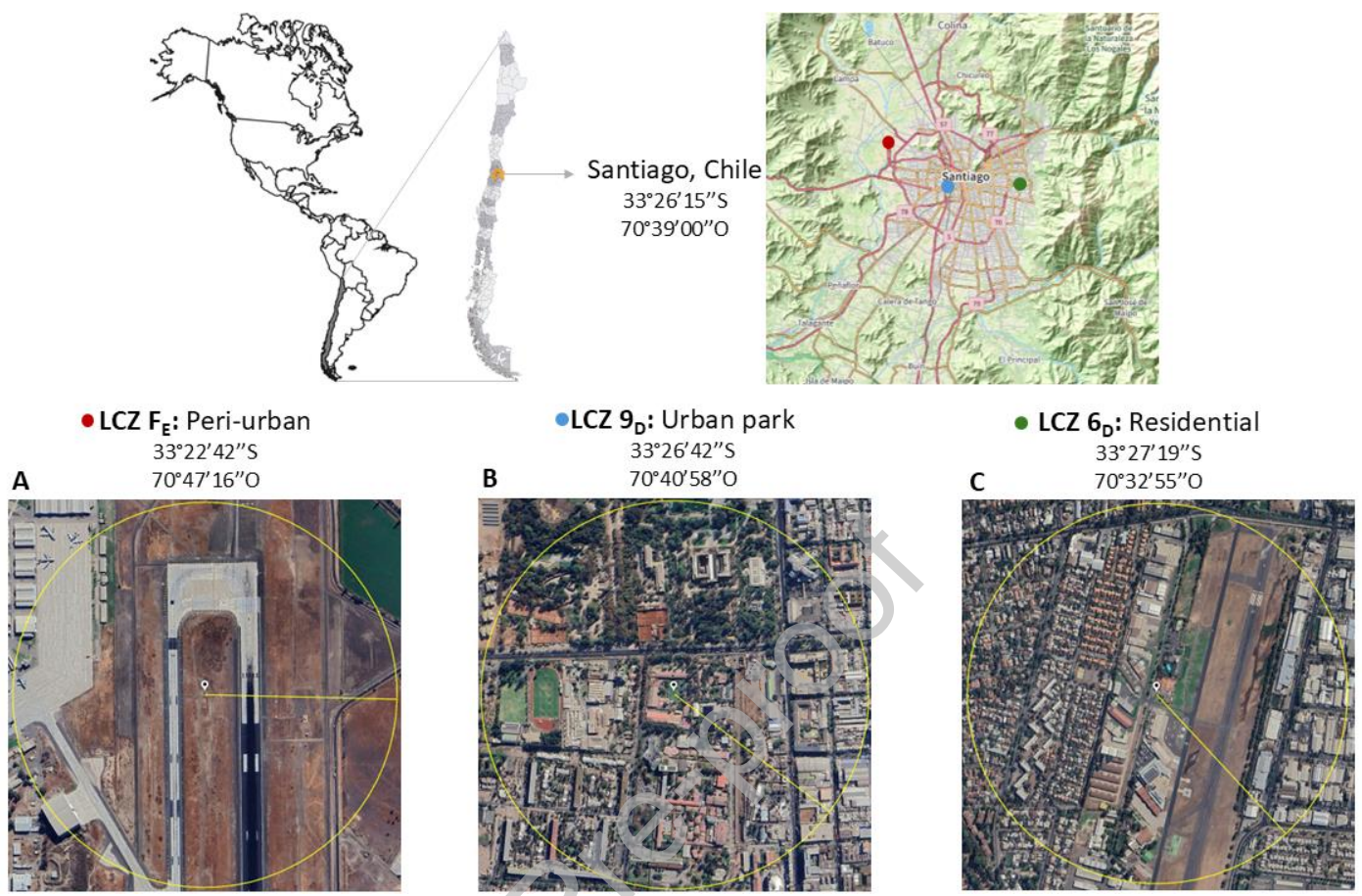


Fig. 2. Location of Chile in South America and administrative map of Chile with the location of its capital, Santiago. Relief of Santiago and its mountainous surroundings (OpenStreetMap, 2025). Satellite images of the three LCZs of study: (A) Peri-urban, (B) Urban park and (C) Residential (Google Earth Pro, 2025).

2.4. Air temperature and rainfall data

Near-surface air temperature available data (at a height of 1.5 m (DMC, 2024)) from 1961 to 2024 was accessed for the three Santiago weather stations. The data from 1961 to 1970 was available at an annual average resolution, and this 10-year period served as the baseline for calculating temperature anomalies after 1971. The data from 1971 to 1980 and from 1981 to 2024 were available at a monthly average and daily average resolution, respectively, and were used to calculate the annual average. The long-term trend was investigated from 1971 onwards.

The annual minimum and maximum temperature averages and the daily temperature range (DTR) were examined to study the long-term trends of these values. The temporal resolution of these data, from 1961 to 2023, was the annual average.

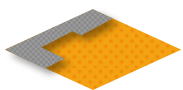
Rainfall data (annually and monthly) were similarly sourced from the three Santiago weather stations from 1961 onwards.

2.5. Satellite observations for land cover change

Satellite imagery of the three sites (LCZ F_E, LCZ 9_D and LCZ 6_D) was analysed to identify potential land cover changes surrounding each weather station from 2000 and 2024 (Table 1), such as in a few cases that have been investigated (Jones et al., 2008). Due to the satellite spatial resolution prior to 2000, it was not possible to accurately calculate the properties in the LCZs.

The survey indicated no significant land-use changes in the urban park (LCZ 9_D) and residential areas (LCZ 6_D) but an increase in the impervious surface in the peri-urban area (LCZ F_E). Beyond the boundary of this last area, within a 2-kilometre radius, there was a reduction in bare soil (LCZ F) and tree cultivation (LCZ B), which was replaced by large, low-rise buildings without vegetation (LCZ 8) and paved areas for aircraft operations (LCZ E) from 2006 onwards.

Table 1. Values of geometric and surface cover properties for LCZs from 2000 to 2024 study period. All properties are unitless except the height of roughness elements. Land cover is calculated within a 500-meter radius surrounding each weather station.

Parameters	Peri-urban	Urban park	Residential	
	LCZ	LCZ F_E	LCZ 9_D	
Representation				
Sky view factor ^a	1.00	>0.6	>0.3	
Canyon (or building) aspect ratio ^b	-	0.1-0.7	0.1-0.3	
Mean vegetation height (m) ^c	<0.25	20.3	7.70	
Mean building height (m) ^d	-	8.80	5.70	
Terrain roughness class ^e	1	5-6	6	
2000 (year)				
Impervious building surface fraction (%) ^f	-	15.6	21.5	
Impervious ground surface fraction (%) ^g	14.8	9.0	20.9	
Pervious surface fraction (%) ^h	85.2	75.4	57.6	
2024 (year)				
Impervious building surface fraction (%) ^f	-	18.3	22.8	
Impervious ground surface fraction (%) ^g	33.3	13.0	24.9	
Pervious surface fraction (%) ^h	66.7	68.7	52.3	

^aRatio of the amount of sky hemisphere visible from ground level to that of an unobstructed hemisphere (Stewart & Oke, 2012).

^bMean height-to-width ratio of street canyons or building spacing.

^cGeometric average of tree heights.

^dGeometric average of buildings heights.

^eEffective terrain roughness Z_0 classification by (Davenport et al., 2000).

^fRatio of impervious building plan area to total plan area.

^gRatio of impervious ground plan area to total plan area (paved surface).

^hRatio of pervious plan area to total plan area (bare soil, vegetation, water).

2.6. Time series analysis of long-term temperature data

2.6.1. Regression analysis

The regression analysis has been used to estimate trends in climate equations analysis (Mudelsee, 2014). The general climate equation is:

$$X(i) = X_{trend}(i) + S(i) \times X_{noise}(i) \quad (1)$$

Eq. (1) decomposes the climate data, $X(i)$, into a trend component and a noise component, where the latter has a mean of zero. The trend, $X_{trend}(i)$, is a key focus in climatology as it describes the mean state of the system, and $S(i)$ quantifies the variability around the trend.

The linear regression describes $X_{trend}(i)$ using two parameters: the intercept, β_0 , and the slope, β_1 . The model is:

$$X(i) = \beta_0 + \beta_1 \times T(i) + S(i) \times X_{noise}(i) \quad (2)$$

$T(i)$ is the time variable assigned to $X(i)$. Since this statistical model uses parameters, the output is in the form of estimated parameter values with an uncertainty measure.

2.6.2. Seasonal time series model

A time series Z_t comprises trend-cycle (P_t), seasonal (S_t), and irregular components (e_t), which can be represented as an additive seasonal model in the form (Wei, 2019):

$$Z_t = P_t + S_t + e_t = \alpha_0 + \sum_{i=1}^m \alpha_i U_{it} + \sum_{j=1}^k \beta_j V_{jt} + e_t \quad (3)$$

where $P_t = \alpha_0 + \sum_{i=1}^m \alpha_i U_{it}$, and the U_{it} are the trend-cycle variables; $S_t = \sum_{j=1}^k \beta_j V_{jt}$, and the V_{jt} are the seasonal variables. The coefficients α and β are regression parameters. The trend-

cycle component P_t captures the long-term evolution of the series, indicating the overall direction over time, while the seasonal component S_t reflects regular short-term fluctuations (e.g., monthly patterns). The irregular component e_t accounts for random noise or unexplained variations. This model helps identify the different influences on the data with an uncertainty level described by mean absolute percentage error (MAPE).

2.6.3. Standardised anomalies

The standardised anomaly z is calculated by subtracting the sample mean \bar{x} from raw data x and dividing by the corresponding sample standard deviation s_x , yielding a normalised, dimensionless quantity:

$$z = \frac{x - \bar{x}}{s_x} = \frac{x'}{s_x} \quad (4)$$

In atmospheric science, an anomaly x' refers to the deviation of a data value from a relevant average and does not imply that the value is abnormal or unusual (Wilks, 2019).

2.7. Statistical analysis

To assess the consistency of the evaluation results, an analysis of variance (ANOVA) was performed to determine the significance of the regression analysis related to inter-annual variations. Additionally, due to the variability of rainfall and the seasonal pattern of temperature, Spearman's rank correlation coefficient was applied to examine the relationships among these two variables and the fraction of pervious surface at a monthly temporal resolution, thereby

addressing correlations in the intra-annual variations. Both statistical analyses were conducted with statistical significances defined at $P<0.05$, $P<0.01$ and $P<0.001$.

3. RESULTS

This section is structured around the research questions of this study, analysing the inter- and intra-annual variability of temperature and precipitation in each LCZ.

3.1. Time evolution of the air temperature and rainfall observations: inter-annual variations

3.1.1. Air temperature anomalies and rainfall trends

A significant warming trend was observed from 1971 onwards, with considerable variation in the rate of warming among the three LCZs (Fig. 3). The linear trend from 1971 to 2023 was most pronounced in the peri-urban area ($0.36\text{ }^{\circ}\text{C}$ per decade), exceeding those in the urban park ($0.21\text{ }^{\circ}\text{C}$ per decade) and residential areas ($0.30\text{ }^{\circ}\text{C}$ per decade). This pattern persisted in the most recent period (2000–2023) with the warming rate in the peri-urban area nearly doubling compared to the entire study period, while the residential area exhibited a moderate increase. In the urban park, however, the warming trend remained consistent across the two periods.

Concurrently, inter-annual rainfall variability differed among the three LCZs, with a decreasing trend evident in recent years (Fig. 4). Prior to 2006, the peri-urban area exhibited substantial variability, with years of well-above-average and well-below-average rainfall. After 2006, however, very wet seasons disappeared, and below-average rainfall events became more frequent. The urban park and residential areas initially displayed similar patterns to the peri-urban area.

Towards the end of the period, the increase in below-average rainfall was less marked in the urban park and residential areas.

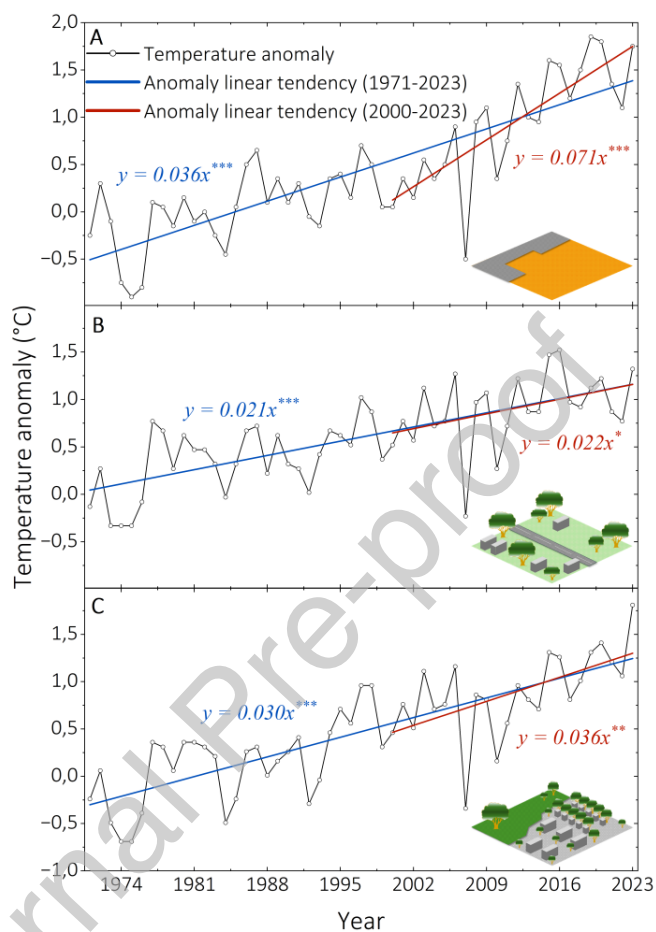


Fig. 3. Average annual temperature anomalies (°C) from original data (black line) with the linear trends for two distinct periods (blue and red lines) for the (A) peri-urban, (B) urban park, and (C) residential areas. Significance reported from the Anova test in linear fitting for each tendency is indicated by asterisks (* indicates $p < 0.05$, ** indicates $p < 0.01$, and *** indicates $p < 0.001$).

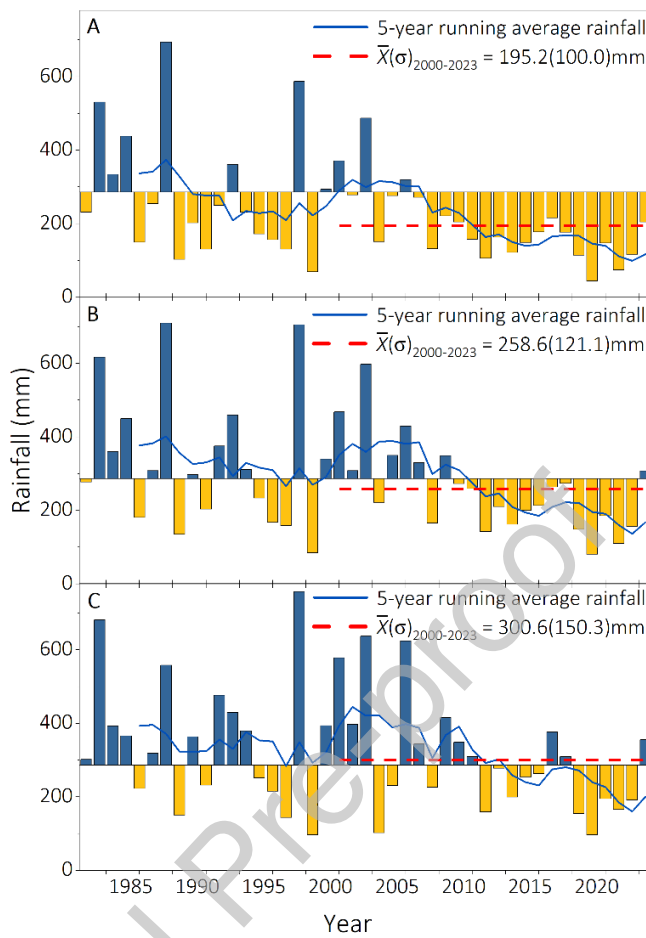


Fig. 4. Time series of annual rainfall (mm) data for the (A) peri-urban, (B) urban park, and (C) residential areas. Blue and yellow bars represent rainfall above and below the average of the 1961-1980 reference period (286.2 mm; DMC, 2024), respectively. Red horizontal dashed line represents the 2000-2023 average rainfall for each area. The average value is shown in the top-right corner of each plot, with the corresponding period's standard deviation shown inside the parentheses.

3.1.2. Minimum and maximum temperatures and daily temperature range trends

The warming rates of minimum and maximum temperatures showed significant variability across the LCZs, resulting in differing trends in the DTR (Fig. 5). In the peri-urban area, a greater increase

in minimum temperatures compared to maximum temperatures led to a negative but no-significant DTR trend. Similarly, the residential area exhibited a no-significant DTR trend but positive. Both areas presented gradients are far less than $\pm 1\%$. Conversely, the urban park area has a significantly greater increase in maximum temperatures compared to the minimum temperatures, resulting in a positive DTR trend.

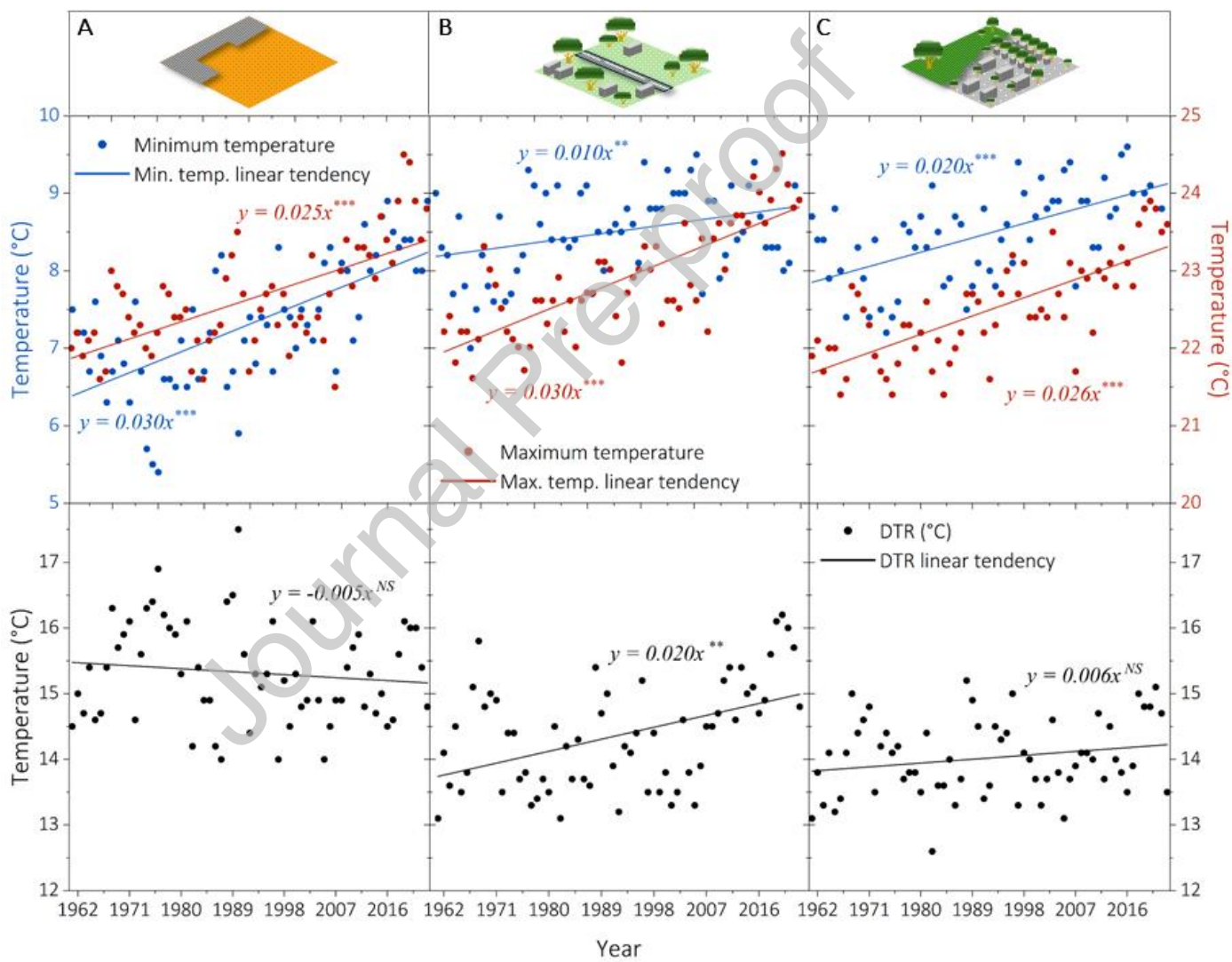


Fig. 5. Annual average minimum, maximum, and DTR temperature data ($^{\circ}\text{C}$) with linear tendencies differentiated by blue, red, and black dots and lines for the (A) peri-urban, (B) urban park, and (C) residential areas, respectively. Significance reported from the Anova test in linear fitting for each tendency is indicated by asterisks (* indicates $p < 0.05$, ** indicates $p < 0.01$, and *** indicates $p < 0.001$). NS indicates no-significance.

3.2. *Intra-annual variations of air temperature and rainfall observations*

Fig. 6 illustrates the average and standard deviation of temperature, irregular variations of temperature and rainfall variability in the annual cycle for the period of study of the peri-urban area. July (winter), the雨iest and second coldest month, exhibits the most irregular temperature variations. In contrast January (summer), the warmest and least rainy month, experiences the least irregular temperature variations. November, although it presents an intermediate temperature and rainy intensity concerning the other months, shows great irregular temperature variations.

Fig. 7 depicts the temporal evolution of monthly rainfall in the peri-urban area, showing a clear decrease towards the end of the analysed period (Box A1). Boxes A2 and A3 of Fig. 7 show the standardised difference in temperature between the three LCZs. For the first two-thirds of the analysed period, temperature changes were more pronounced in the urban park and residential areas. Towards the end of the period, greater temperature changes were observed in the peri-urban area.

In line with the above, the peri-urban area also experienced the most notable land cover change between 2000 and 2024, particularly a reduction in the proportion of pervious surfaces, as shown in Table 1. Consequently, Table 2 presents the results of the Spearman's rank correlation analysis, which examines the correlation of monthly temperature against rainfall and pervious surface fraction data. The analysis reveals a statistically significant negative correlation ($r < 0$, $p < 0.001$) between monthly temperature and rainfall data.

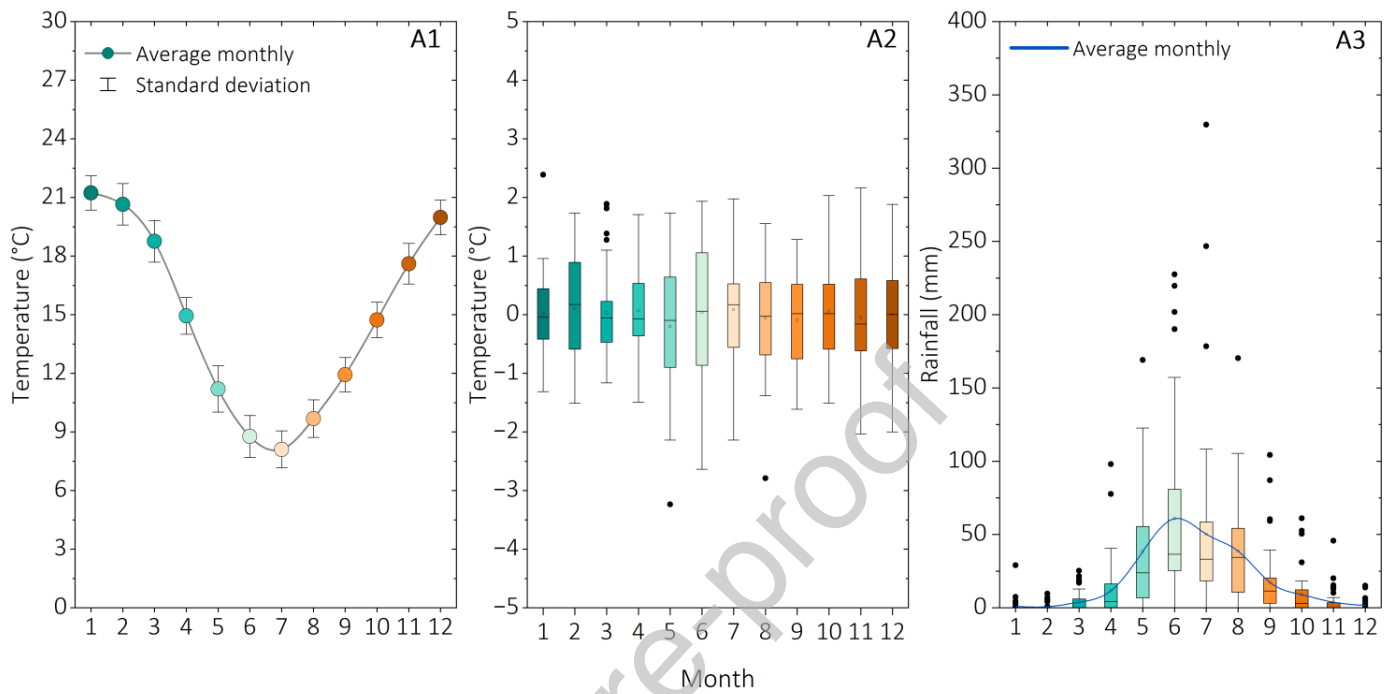


Fig. 6. Monthly temperature average and its standard deviation ($^{\circ}\text{C}$) (A1), irregular temperature ($^{\circ}\text{C}$) variations per month obtained by the time series model with a MAPE value of 5.32% (A2), and monthly rainfall (mm) data (A3) are represented in the peri-urban area from January 1981 to July 2024. Each colour represents each month for the analysis period.

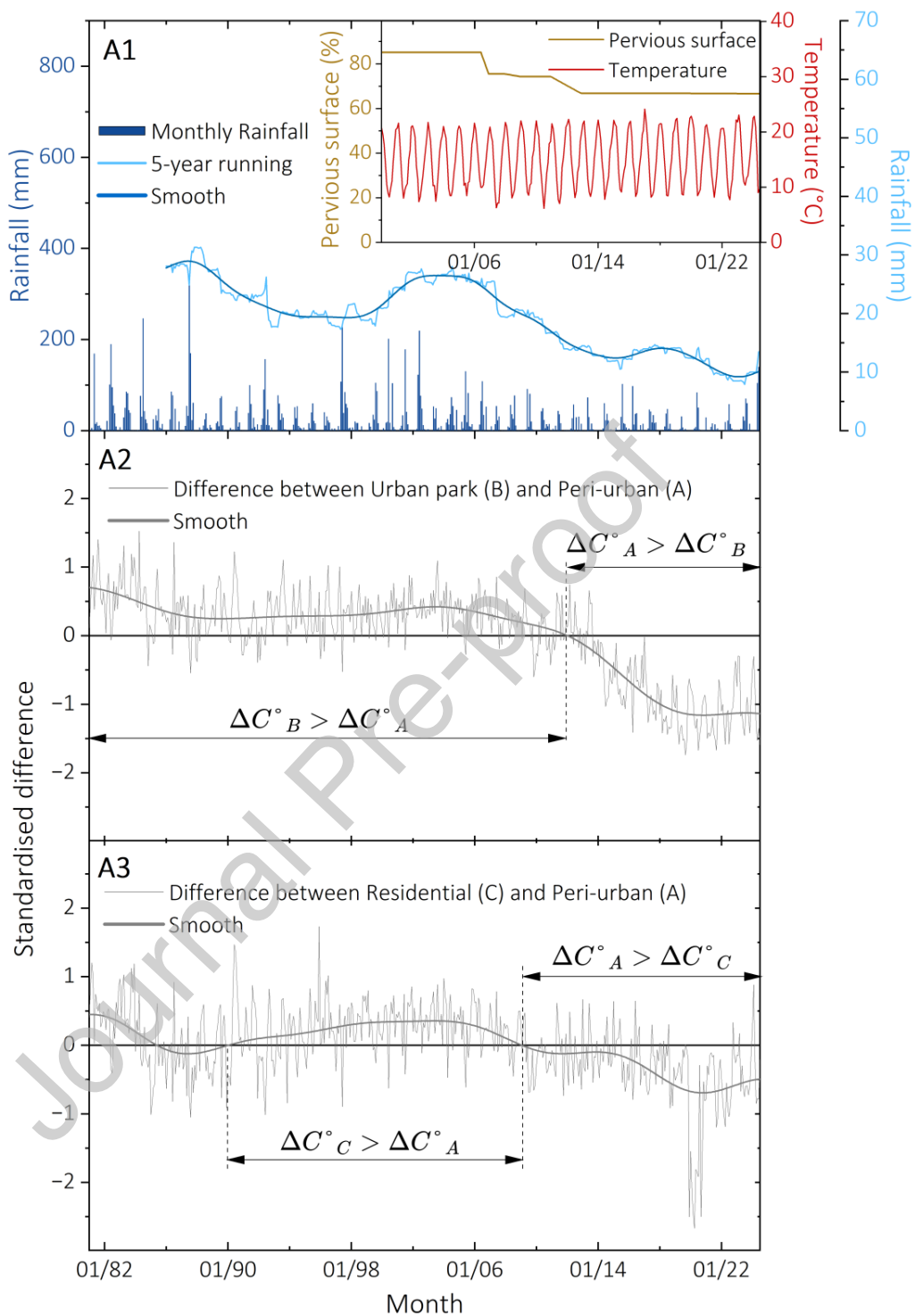


Fig. 7. Monthly average rainfall (mm), 5-year running monthly average rainfall (mm), pervious surface (%), and temperature (°C) in the peri-urban area (**A1**) are represented by dark blue bars (y-axis to the left), light blue lines (y-axis to the right), bronze yellow line (mini-box y-axis to the left), and red line (mini-box y-axis to the right),

respectively. Standardised differences in monthly air temperature between the urban park and peri-urban area (**A2**), and between residential and peri-urban areas (**A3**) from January 1981 to July 2024. Both the 5-year running monthly average rainfall and standardised differences were smoothed using Fourier harmonics to capture variables' modest but obvious deviations from a single sine wave. The standardised differences, Δz , were calculated by subtracting the standardised anomalies of each location (Eq. 3), where $\Delta z = z_x - z_y$ for each month in the study period. This ensures that the resulting index will have a unit standard deviation.

Table 2. Spearman rank correlation between monthly average temperature (°C), rainfall (mm) and pervious surface (%) data in the peri-urban area (r values) from January 2000 to July 2024. Asterisks indicate statistical significance for each relationship (* indicates $p < 0.05$, ** indicates $p < 0.01$, and *** indicates $p < 0.001$). NS indicates no-significance.

Spearman rank correlation coefficients			
Variables	Temperature	Rainfall	Pervious surface
Temperature	1.00 ***	-0.73 ***	-0.093 NS

4. DISCUSSION

4.1. *Inter-annual air temperature and rainfall variability*

The analysis of urban time series data provides valuable insights into historical climate trends and the potential influence of urbanisation on these patterns (Masson et al., 2020). While global climate change exhibits regional variability in trends and risks (Cleugh & Grimmond, 2012), its effects on the urban scale show significant variation in air temperature response and rainfall variability on both inter- and intra-annual timescales. Our investigation of urban air temperature trends in a valley city with a semi-arid climate and their relationship with rainfall variability due to

climate change revealed discrepancies in the warming rate over the entire study period (1971–2023) and the recent years (2000–2023). The peri-urban area (LCZ F_E) presented the highest warming rate during the entire period (0.36°C per decade), and it worsened in recent years by increasing by 97% to 0.71 °C per decade under conditions of well-below-average rainfall. While this increasing air temperature trend in recent decades in this area could be linked to the accelerated global warming (Forster et al., 2024; WMO, 2024), this hypothesis was discarded since the warming rate in the urban park and residential areas remained almost consistent across the two periods and did not show similar recent increases.

Drought conditions in central Chile, where Santiago is located, have been extensively reported (Garreaud et al., 2020; Peña-Guerrero et al., 2020). Decreased soil moisture affects its thermal inertia, modulating the surface-atmosphere thermal interaction (Martilli et al., 2020). Such conditions are consistent with environmental patterns where higher temperatures are associated with drier soil (Chen et al., 2025; Lanet et al., 2024), as these influence the surface energy balance by increasing sensible heat while latent heat is reduced (Oke et al., 2017). This validates our hypothesis since the peri-urban area, characterised by a permeable surface (predominantly bare soil) and minimal impermeable surface, exhibited a stronger warming response to changes in rainfall and drought. This puts peri-urban areas of Santiago on alert to the increase in warming rate compared with reports in other semi-arid and arid urban areas (Pingale et al., 2014).

The urban park weather station showed a smaller decrease in precipitation compared to the peri-urban area and the lowest warming rate. There are two conditions under which the warming rate is little altered by decreasing rainfall in this area: i) well-irrigated conditions (Reyes-Paecke et al., 2019) that largely maintain the energy balance during dry periods and ii) the surrounding

impermeable surfaces, predominantly dense, low-rise buildings and paved surfaces, which remain substantially unaffected by drought as their thermal properties are not influenced by the lack of moisture. Similarly, the residential area has a combination of impermeable and permeable surfaces but contains more vegetation cover, sustained through residential irrigation during the whole year at a fairly constant rate (Sanzana et al., 2019). This irrigation mitigates the effects of droughts and supports evaporative cooling, significantly reducing air temperatures and increasing atmospheric water content. As a result, it enhances the 'oasis effect,' where advected energy from hotter, drier surrounding areas influences the irrigated areas (Vivoni et al., 2020).

Climate change also affects the DTR trends, which are related to the thermal interactions between the surface and the atmosphere (Martilli et al., 2020). Due to the contrasting urban surfaces analysed in this study, different DTR trends were obtained, explained by the variability of trends in maximum and minimum temperatures. The maximum temperature trends in the three areas were similar (0.27°C per decade on average), driven primarily by regional warming rather than precipitation changes. However, it is important to note that the urban park exhibited the highest rate of warming of maximum temperature (0.30°C per decade), slightly above the other areas. This is possibly due to advection processes that transport warm air masses from the surrounding large concrete surfaces and buildings (Yan et al., 2018) influencing the measured temperatures.

Differently, minimum temperatures showed disparities, leading to a difference of 0.20°C per decade between the three LCZs. Climate change-induced rainfall reduction and higher temperatures due to global warming led to prolonged periods of dry soil (Stolpe & Undurraga, 2016). Unlike wet and saturated soils, a dry soil has significantly lower heat capacity, it cools

down quickly at night and heats up rapidly in the morning. Impermeable surfaces such as concrete and asphalt, however, store more heat during the day due to higher thermal inertia than soil, and they released it at night as infrared energy. The thermal characteristics of these two surfaces explain why the peri-urban area had the highest increase in minimum temperatures. Conversely, the urban park area exhibited the lowest increase in minimum temperatures, followed by the residential area. Here, again, the well-irrigated conditions in both areas allowed the minimum temperature trends to be most linked to regional warming. So far, these partial results highlight the role of permeable surfaces in regulating temperature trends due to moisture changes, addressing the study's first research question focused on inter-annual air temperature trends in the context of climate change.

4.2. Intra-annual temperature and rainfall variability

Whereas prior studies have quantified the impact of climate change on urban warming in terms of inter-annual variability (Ajaaj et al., 2018; Arsiso et al., 2018; Pingale et al., 2014), our investigation delves deeper into exploring its implications for intra-annual variability. Specifically, regarding irregular temperature variations in the peri-urban area the most affected LCZ by rainfall decreases our analysis demonstrates that the high rainfall variability during the coldest months exerted more pronounced irregular variations during these months. This occurs through changes in evaporative cooling due to the permeable surface conditions. However, a similar effect is observed in the final months of the annual cycle, during which the drying effect, driven by a weakened water vapour source (i.e., reduced rainfall), further amplifies irregular variations.

Considering this intra-annual variability over the long study period, the standardised anomaly method provided further insight. Using the peri-urban area as a reference, we observed that temperature changes were primarily concentrated in the urban park and residential areas at the beginning of the study period. Rainfall was variable but did not decrease in this first part. However, towards the end of the period, a progressive decline in rainfall intensity led to significant alterations in the air temperature in the peri-urban area, largely attributed to soil drying. It is important to note a significant reduction of 18.5% in the pervious surface for this area. According to the Spearman rank analysis, the correlation between monthly temperature and pervious surface data was very low (-0.093), with an absence of a statistically significant correlation.

Monthly (intra-annual) and yearly (inter-annual) fluctuations in rainfall were key to understanding the internal temperature variability of each LCZ, in which the peri-urban area established a clear precedent: its temperature can fluctuate significantly from year to year and month to month compared to other areas due to its permeable bare soil surface conditions, as previously highlighted. The results of intra-annual variability not only strengthen the validation of our hypothesis but also address the second research question of how the intra-annual temperature variability differs in response to climate change for the three contrasting LCZs.

4.3. Recommendations and future lines

The results of this study indicate that temperature variations within all three LCZs are not only possible on annual and monthly scales, but they are virtually inevitable to occur due to their intrinsic conditions. This underscores the need to move beyond simplistic urban-rural

comparisons and adopt methodologies such as the LCZ approach to better understand urban-atmosphere interactions (Martilli et al., 2020). As global temperatures continue to rise due to increasing greenhouse gas emissions, we caution that temperature variability within each LCZ, driven by their surface conditions, is expected to persist in response to the accelerating rate of global warming.

Our study combined temperature, rainfall and land cover data to assess the impact of climate change on a valley city characterised by a semi-arid climate. However, a more comprehensive evaluation of climate change in urban environments requires the inclusion of additional environmental parameters, such as wind speed and direction. Future investigations into urban air temperature could benefit from integrating in-situ observations with high-resolution urban climate models, allowing for a more complete analysis that incorporates these environmental variables alongside land-use changes, using the LCZ classification framework. Moreover, incorporating data on vegetation decline provides a more holistic understanding of urban warming trends associated with urban browning (widespread vegetation loss).

Urgent measures to combat soil drying caused by decreased rainfall are needed since it can induce urban browning due to water shortages in central Chile (Meza et al., 2014). Zhang et al. (2021) observed a predominantly negative vegetation trend across South America from 2000 to 2018. Similarly, Du et al. (2025) recently analysed the urban browning phenomenon in cities across the Global South, finding that Santiago is affected, with temperature rising 0.05 °C per decade due to this process.

We strongly recommend that urban planners and governments prioritise the control of vegetation loss, particularly in biophysically (urban greenness) and socio-economically vulnerable

areas. Such loss can exacerbate air warming through reduced evaporative cooling, more so than through its drying caused by a weakened water vapour source (Du et al., 2025). For instance, urban forestry can be sustained by integrating traditional practices with emerging technologies to enhance resilience against drought and high temperatures (Esperon-rodriguez et al., 2025). National and local governments must share the responsibility of supporting disadvantaged urban areas, which often lack the resources for greening initiatives (Ju et al., 2023) and rainwater harvesting systems for irrigation (Eisenman et al., 2025). This is particularly urgent in many arid and semi-arid cities where water security is critical and unsustainable practices persist (Di Baldassarre et al., 2018). Furthermore, economically constrained communities may benefit from cost-effective strategies such as public awareness campaigns, educational materials on urban gardening, and the distribution of low-cost seedlings to promote local vegetation efforts (Puskás et al., 2021).

4.4. Methodological limitations

In an urban context characterised by significant heterogeneity, achieving an accurate temperature measurement that fully represents all spatial and surface features is inherently challenging. Temperature measurements within the urban canopy that adhere to the standard requirements for urban measurement siting (Oke, 2006) can be difficult to obtain due to the pronounced spatial variability of the temperature field. The LCZ methodology developed by Stewart & Oke (2012) allows direct comparison of point temperature measurements as a spatial average over a 500-meter radius or less. Point measurements remain a valuable means of representing air temperature in response to climatic factors and surface energy balance,

particularly for configurations that are not yet fully understood. This principle underpins the use of models which rely on physical principles to reflect our current understanding of how the atmosphere interacts with the Earth's surface. In this regard, the use of weather meteorological stations served two critical purposes in this research. First, the stations, which are managed by government meteorological entities, follow the parameters and recommendations of the World Meteorological Organization (WMO), ensuring high-quality measurements. Second, the long-term operation of these stations, spanning several decades, enabled us to investigate the impact of climate change in a semi-arid urban area and assess how its responses vary depending on urban surface characteristics. These long-term datasets were essential for identifying the complex interactions between rainfall variability, surface permeability, and temperature trends, ultimately strengthening the robustness of our findings and advancing research in urban valley climates and conditions.

5. CONCLUSIONS

This study identified varying long-term temperature trends in Santiago, Chile, driven by global warming and rainfall variability due to climate change across three distinct LCZ scenarios. The peri-urban area (LCZ F_E), characterised by permeable surfaces (e.g. bare soil), exhibited the highest inter-annual warming rate and intra-annual temperature variations due to prolonged drought periods in comparison to the urban park (LCZ 9_D) and residential (LCZ 6_D) areas. However, these last two areas initially showed slightly greater temperature variations in the intra-annual analysis. As rainfall progressively declined, temperature increases became more pronounced in the peri-urban area (0.71 °C per decade) towards the end of the study period

compared to urban park (0.22°C per decade) and residential areas (0.36°C per decade). The well-irrigated permeable surfaces in the urban park exhibited more stable thermal conditions, limiting significant temperature fluctuations despite rainfall changes. Meanwhile, the residential area benefited from abundant vegetation and well-irrigated conditions, mitigating climate change effects. Future research should prioritise local-scale comparisons using the LCZ methodology to enhance understanding of urban surface-atmosphere interactions rather than relying on simplistic urban-rural differences that underpin urban heat island reporting. Furthermore, climate change mitigation policies in Santiago should focus on quantifying impacts at the neighbourhood scale rather than at citywide or regional levels, particularly in light of the increasing drought in this semi-arid region and the accelerating pace of global warming. It calls for more comprehensive research that includes variables like wind and urban browning, and urges urban planners to prioritise vegetation management, especially in vulnerable areas, to mitigate urban warming and strengthen climate resilience in semi-arid cities.

REFERENCES

Ajaaj, A. A., Mishra, A. K., & Khan, A. A. (2018). Urban and peri-urban precipitation and air temperature trends in mega cities of the world using multiple trend analysis methods. *Theoretical and Applied Climatology*, 132(1–2), 403–418. <https://doi.org/10.1007/s00704-017-2096-7>

Aldunce, P., Araya, D., Sapiain, R., Ramos, I., Lillo, G., Urquiza, A., & Garreaud, R. (2017). Local Perception of Drought Impacts in a Changing Climate: The Mega-Drought in Central Chile. *Sustainability*, 9(11), 2053. <https://doi.org/10.3390/su9112053>

Arsiso, B. K., Mengistu Tsidu, G., & Stoffberg, G. H. (2018). Signature of present and projected climate change at an urban scale: The case of Addis Ababa. *Physics and Chemistry of the Earth*, 105(March), 104–114. <https://doi.org/10.1016/j.pce.2018.03.008>

Bayer-Altin, T., Sadykova, D., & Türkeş, M. (2024). Evolution of long-term trends and variability in air temperatures of Kazakhstan for the period 1963–2020. *Theoretical and Applied Climatology*, 155(1), 541–566. <https://doi.org/10.1007/s00704-023-04650-7>

Beck, H. E., Zimmermann, N. E., McVicar, T. R., Vergopolan, N., Berg, A., & Wood, E. F. (2018). Present and future Köppen-Geiger climate classification maps at 1-km resolution. *Scientific Data*, 5(1), 180214. <https://doi.org/10.1038/sdata.2018.214>

Bonacci, O., & Đurin, B. (2023). The Behavior of Diurnal Temperature Range (DTR) and Annual Temperature Range (ATR) in the Urban Environment: A Case of Zagreb Grič, Croatia. *Atmosphere*, 14(9), 1346. <https://doi.org/10.3390/atmos14091346>

Chen, X., Wang, J., Pan, F., Song, Y., Liang, J., Huang, N., Jiang, K., Gao, R., Men, J., Bi, P., Zhang, F., Huang, Z., Huang, B., & Pan, Z. (2025). Land-atmosphere feedback exacerbated the mega heatwave and drought over the Yangtze River Basin of China during summer 2022. *Agricultural and Forest Meteorology*, 361, 110321. <https://doi.org/10.1016/j.agrformet.2024.110321>

Cleugh, H., & Grimmond, S. (2012). Urban Climates and Global Climate Change. In *The Future of the World's Climate* (pp. 47–76). Elsevier. <https://doi.org/10.1016/B978-0-12-386917-3.00003-8>

Di Baldassarre, G., Wanders, N., AghaKouchak, A., Kuil, L., Rangecroft, S., Veldkamp, T. I. E., Garcia, M., van Oel, P. R., Breinl, K., & Van Loon, A. F. (2018). Water shortages worsened by

reservoir effects. *Nature Sustainability*, 1(11), 617–622. <https://doi.org/10.1038/s41893-018-0159-0>

DMC. (2024). *Online Database of Meteorological Information*.

<https://climatologia.meteochile.gob.cl/>

Dodman, D., Hayward, B., Pelling, M., Castán Broto, V., Chow, W., Chu, E., Dawson, R., Khirfan, L., McPhearson, T., Prakash, A., Zheng, Y., & Ziervogel, G. (2023). Cities, Settlements and Key Infrastructure. In H. O. Pörtner, M. Roberts, E. . Poloczanska, K. Mintenbeck, M. Alegría, M. Craig, S. Langsdorf, S. Löschke, V. Möller, A. Okem, & B. Rama (Eds.), *Climate Change 2022 – Impacts, Adaptation and Vulnerability* (pp. 907–1040). Cambridge University Press.

<https://doi.org/10.1017/9781009325844.008>

Du, H., Zhan, W., Zhou, B., Ju, Y., Liu, Z., Middel, A., Huang, K., Zhao, L., Chakraborty, T., Wang, Z., Wang, S., Li, J., Li, L., Huang, F., Ji, Y., Li, X., & Li, M. (2025). Exacerbated heat stress induced by urban browning in the Global South. *Nature Cities*. <https://doi.org/10.1038/s44284-024-00184-9>

Eisenman, T. S., Roman, L. A., Östberg, J., Campbell, L. K., & Svendsen, E. (2025). Beyond the Golden Shovel. *Journal of the American Planning Association*, 91(1), 133–143. <https://doi.org/10.1080/01944363.2024.2330943>

Esperon-rodriguez, M., Gallagher, R., Calfapietra, C., Cariñanos, P., Dobbs, C., Eleuterio, A. A., Rodriguez, D. E., Jahani, A., & Litvak, E. (2025). Barriers and opportunities for resilient and sustainable urban forests. *Nature Cities*, 2(April), 290–298. <https://doi.org/10.1038/s44284-025-00212-2>

Forster, P. M., Smith, C., Walsh, T., Lamb, W. F., Lamboll, R., Hall, B., Hauser, M., Ribes, A., Rosen,

D., Gillett, N. P., Palmer, M. D., Rogelj, J., von Schuckmann, K., Trewin, B., Allen, M., Andrew, R., Betts, R. A., Borger, A., Boyer, T., ... Zhai, P. (2024). Indicators of Global Climate Change 2023: annual update of key indicators of the state of the climate system and human influence. *Earth System Science Data*, 16(6), 2625–2658. <https://doi.org/10.5194/essd-16-2625-2024>

Garreaud, R. D., Boisier, J. P., Rondanelli, R., Montecinos, A., Sepúlveda, H. H., & Veloso-Aguila, D. (2020). The Central Chile Mega Drought (2010–2018): A climate dynamics perspective. *International Journal of Climatology*, 40(1), 421–439. <https://doi.org/10.1002/joc.6219>

Gauthier, T. D. (2001). Detecting Trends Using Spearman's Rank Correlation Coefficient. *Environmental Forensics*, 2(4), 359–362. <https://doi.org/10.1080/713848278>

Google Earth Pro. (2025). *Santiago, Chile. 33°26'15"S 70°39'00"O, Eye alt. 2.60 km (V 7.3.6.9796)*. Airbus 2025. <http://www.earth.google.com>

Hall, S. J., Learned, J., Ruddell, B., Larson, K. L., Cavender-Bares, J., Bettez, N., Groffman, P. M., Grove, J. M., Heffernan, J. B., Hobbie, S. E., Morse, J. L., Neill, C., Nelson, K. C., O'Neil-Dunne, J. P. M., Ogden, L., Pataki, D. E., Pearse, W. D., Polsky, C., Chowdhury, R. R., ... Trammell, T. L. E. (2016). Convergence of microclimate in residential landscapes across diverse cities in the United States. *Landscape Ecology*, 31(1), 101–117. <https://doi.org/10.1007/s10980-015-0297-y>

Hobbie, S. E., & Grimm, N. B. (2020). Nature-based approaches to managing climate change impacts in cities. *Philosophical Transactions of the Royal Society B: Biological Sciences*, 375(1794), 20190124. <https://doi.org/10.1098/rstb.2019.0124>

INE. (2019). *Estimaciones y proyecciones de la población de chile 2002-2035 totales regionales*,

población urbana y rural. INE Chile.

Irizarry-Ortiz, M. M., Obeysekera, J., Park, J., Trimble, P., Barnes, J., Park-Said, W., & Gadzinski, E. (2013). Historical trends in Florida temperature and precipitation. *Hydrological Processes*, 27(16), 2225–2246. <https://doi.org/10.1002/hyp.8259>

Jones, P. D., Lister, D. H., & Li, Q. (2008). Urbanization effects in large-scale temperature records, with an emphasis on China. *Journal of Geophysical Research Atmospheres*, 113(16), 1–12. <https://doi.org/10.1029/2008JD009916>

Joshi, M. Y., Rodler, A., Musy, M., Guernouti, S., Cools, M., & Teller, J. (2022). Identifying urban morphological archetypes for microclimate studies using a clustering approach. *Building and Environment*, 224, 109574. <https://doi.org/10.1016/j.buildenv.2022.109574>

Ju, Y., Dronova, I., Rodriguez, D. A., Bakhtsiyarava, M., & Farah, I. (2023). Recent greening may curb urban warming in Latin American cities of better economic conditions. *Landscape and Urban Planning*, 240, 104896. <https://doi.org/10.1016/j.landurbplan.2023.104896>

Koudahe, K., Kayode, A. J., Samson, A. O., Adebola, A. A., & Djaman, K. (2017). Trend Analysis in Standardized Precipitation Index and Standardized Anomaly Index in the Context of Climate Change in Southern Togo. *Atmospheric and Climate Sciences*, 07(04), 401–423. <https://doi.org/10.4236/acs.2017.74030>

Lai, L. W., & Cheng, W. L. (2010). Air temperature change due to human activities in Taiwan for the past century. *International Journal of Climatology*, 30(3), 432–444. <https://doi.org/10.1002/joc.1898>

Lanet, M., Li, L., & Le Treut, H. (2024). A framework to assess climate change effects on surface air temperature and soil moisture and application to Southwestern France. *Climatic Change*,

177(12), 170. <https://doi.org/10.1007/s10584-024-03825-z>

Li, D., Malyshev, S., & Shevliakova, E. (2016). Exploring historical and future urban climate in the Earth System Modeling framework: 2. Impact of urban land use over the Continental United States. *Journal of Advances in Modeling Earth Systems*, 8(2), 936–953. <https://doi.org/10.1002/2015MS000579>

Licón-Portillo, J. A., Martínez-Torres, K. E., Chung-Alonso, P., & Herrera Peraza, E. F. (2024). From Block to City Scale: Greenery's Contribution to Cooling the Urban Environment. *Urban Science*, 8(2), 41. <https://doi.org/10.3390/urbansci8020041>

Liu, Z., Lu, G., He, H., Wu, Z., & He, J. (2018). A conceptual prediction model for seasonal drought processes using atmospheric and oceanic standardized anomalies: application to regional drought processes in China. *Hydrology and Earth System Sciences*, 22(1), 529–546. <https://doi.org/10.5194/hess-22-529-2018>

Livada, I., Synnefa, A., Haddad, S., Paolini, R., Garshasbi, S., Ulpiani, G., Fiorito, F., Vassilakopoulou, K., Osmond, P., & Santamouris, M. (2019). Time series analysis of ambient air-temperature during the period 1970–2016 over Sydney, Australia. *Science of the Total Environment*, 648, 1627–1638. <https://doi.org/10.1016/j.scitotenv.2018.08.144>

Martilli, A., Krayenhoff, E. S., & Nazarian, N. (2020). Is the Urban Heat Island intensity relevant for heat mitigation studies? *Urban Climate*, 31(September 2019), 100541. <https://doi.org/10.1016/j.uclim.2019.100541>

Masson, V., Lemonsu, A., Hidalgo, J., & Voogt, J. (2020). Urban Climates and Climate Change. *Annual Review of Environment and Resources*, 45(1), 411–444. <https://doi.org/10.1146/annurev-environ-012320-083623>

McPhee, J., Cortés, G., Rojas, M., Garcia, L., Descalzi, A., & Vargas, L. (2014). Downscaling Climate Changes for Santiago: What Effects can be Expected? In *Climate Adaptation Santiago* (pp. 19–41). Springer Berlin Heidelberg. https://doi.org/10.1007/978-3-642-39103-3_2

Meza, F. J., Vicuña, S., Jelinek, M., Bustos, E., & Bonelli, S. (2014). Assessing water demands and coverage sensitivity to climate change in the urban and rural sectors in central Chile. *Journal of Water and Climate Change*, 5(2), 192–203. <https://doi.org/10.2166/WCC.2014.019>

Mills, T. (2019). *Applied Time Series Analysis*. Elsevier. <https://doi.org/10.1016/C2016-0-03956-6>

Minderlein, S., & Menzel, L. (2015). Evapotranspiration and energy balance dynamics of a semi-arid mountainous steppe and shrubland site in Northern Mongolia. *Environmental Earth Sciences*, 73(2), 593–609. <https://doi.org/10.1007/s12665-014-3335-1>

Moser, A., Uhl, E., Rötzer, T., Biber, P., Caldentey, J., & Pretzsch, H. (2018). Effects of climate trends and drought events on urban tree growth in Santiago de Chile. *Ciencia e Investigación Agraria*, 45(1), 35–50. <https://doi.org/10.7764/rcia.v45i1.1793>

Mudelsee, M. (2014). *Climate Time Series Analysis* (2nd ed., Vol. 51). Springer International Publishing. <https://doi.org/10.1007/978-3-319-04450-7>

Mudelsee, M. (2019). Trend analysis of climate time series: A review of methods. *Earth-Science Reviews*, 190, 310–322. <https://doi.org/10.1016/j.earscirev.2018.12.005>

Ohba, M. (2021). Precipitation under climate change. In *Precipitation* (pp. 21–51). Elsevier. <https://doi.org/10.1016/B978-0-12-822699-5.00002-1>

Oke, T. R. (2006). *Initial Guidance to Obtain Representative Meteorological Observations at Urban Sites. World Meteorological Organization.* <https://books.google.com.au/books?id=xgYxvwEACAAJ>

Oke, T. R., Mills, G., Christen, A., & Voogt, J. A. (2017). *Urban Climates*. Cambridge University Press. <https://doi.org/10.1017/9781139016476>

OpenStreetMap. (2025). *Tracestrack Topo* © OpenStreetMap Contributors.

<https://www.openstreetmap.org/#map=11/-33.4921/-70.6750&layers=P>

Peña-Guerrero, M. D., Nauditt, A., Muñoz-Robles, C., Ribbe, L., & Meza, F. (2020). Drought impacts on water quality and potential implications for agricultural production in the Maipo River Basin, Central Chile. *Hydrological Sciences Journal*, 65(6), 1005–1021. <https://doi.org/10.1080/02626667.2020.1711911>

Pingale, S. M., Khare, D., Jat, M. K., & Adamowski, J. (2014). Spatial and temporal trends of mean and extreme rainfall and temperature for the 33 urban centers of the arid and semi-arid state of Rajasthan, India. *Atmospheric Research*, 138, 73–90. <https://doi.org/10.1016/j.atmosres.2013.10.024>

Piticar, A. (2018). Changes in heat waves in Chile. *Global and Planetary Change*, 169(October 2017), 234–246. <https://doi.org/10.1016/j.gloplacha.2018.08.007>

Privalsky, V. (2023). *Practical Time Series Analysis in Natural Sciences*. Springer International Publishing. <https://doi.org/10.1007/978-3-031-16891-8>

Puskás, N., Abunnasr, Y., & Naalbandian, S. (2021). Assessing deeper levels of participation in nature-based solutions in urban landscapes – A literature review of real-world cases. *Landscape and Urban Planning*, 210, 104065. <https://doi.org/10.1016/j.landurbplan.2021.104065>

Randolph, G. F., & Storper, M. (2023). Is urbanisation in the Global South fundamentally different? Comparative global urban analysis for the 21st century. *Urban Studies*, 60(1), 3–

25. <https://doi.org/10.1177/00420980211067926>

Reyes-Paecke, S., Gironás, J., Melo, O., Vicuña, S., & Herrera, J. (2019). Irrigation of green spaces and residential gardens in a Mediterranean metropolis: Gaps and opportunities for climate change adaptation. *Landscape and Urban Planning*, 182, 34–43. <https://doi.org/10.1016/J.LANDURBPLAN.2018.10.006>

Sanzana, P., Gironás, J., Braud, I., Muñoz, J., Vicuña, S., Reyes-Paecke, S., de la Barrera, F., Branger, F., Rodríguez, F., Vargas, X., Hitschfeld, N., & Hormazábal, S. (2019). Impact of Urban Growth and High Residential Irrigation on Streamflow and Groundwater Levels in a Peri-Urban Semiarid Catchment. *JAWRA Journal of the American Water Resources Association*, 55(3), 720–739. <https://doi.org/10.1111/1752-1688.12743>

Sarricolea, P., Herrera-Ossandon, M., & Meseguer-Ruiz, Ó. (2017). Climatic regionalisation of continental Chile. *Journal of Maps*, 13(2), 66–73. https://doi.org/10.1080/17445647.2016.1259592/SUPPL_FILE/TJOM_A_1259592_SM4818.PDF

Sarricolea, P., Smith, P., Romero-Aravena, H., Serrano-Notivoli, R., Fuentealba, M., & Meseguer-Ruiz, Ó. (2022). Socioeconomic inequalities and the surface heat island distribution in Santiago, Chile. *Science of the Total Environment*, 832(April), 155152. <https://doi.org/10.1016/j.scitotenv.2022.155152>

Shen, Y., & Chen, Y. (2010). Global perspective on hydrology, water balance, and water resources management in arid basins. *Hydrological Processes*, 24(2), 129–135. <https://doi.org/10.1002/hyp.7428>

Snyder, K. A., & Tartowski, S. L. (2006). Multi-scale temporal variation in water availability:

Implications for vegetation dynamics in arid and semi-arid ecosystems. *Journal of Arid Environments*, 65(2), 219–234. <https://doi.org/10.1016/j.jaridenv.2005.06.023>

Stewart, I. (2013). Local climates of the city. *Architectural Design*, 83(4), 100–105. <https://doi.org/10.1002/ad.1625>

Stewart, I. D., & Oke, T. R. (2012). Local Climate Zones for Urban Temperature Studies. *Bulletin of the American Meteorological Society*, 93(12), 1879–1900. <https://doi.org/10.1175/BAMS-D-11-00019.1>

Stolpe, N., & Undurraga, P. (2016). Long term climatic trends in Chile and effects on soil moisture and temperature regimes. *Chilean Journal of Agricultural Research*, 76(4), 487–496. <https://doi.org/10.4067/S0718-58392016000400013>

U.S. Geological Survey. (2025). *EarthExplorer*. Mapping 101. <https://www.usgs.gov/science/science-explorer/maps-and-mapping/mapping-101>

Vivoni, E. R., Kindler, M., Wang, Z., & Pérez-Ruiz, E. R. (2020). Abiotic Mechanisms Drive Enhanced Evaporative Losses under Urban Oasis Conditions. *Geophysical Research Letters*, 47(22). <https://doi.org/10.1029/2020GL090123>

Wei, W. W. S. (2019). *Time Series Analysis: Univariate and Multivariate Methods (Classic Version)*. Pearson Education. https://books.google.com.au/books?id=_v-xswEACAAJ

Wilks, D. S. (2019). *Statistical Methods in the Atmospheric Sciences*. Elsevier. <https://doi.org/10.1016/C2017-0-03921-6>

WMO. (2024). *State of the Global Climate 2023*. <https://library.wmo.int/idurl/4/68835%0A>

Yan, H., Wu, F., & Dong, L. (2018). Influence of a large urban park on the local urban thermal environment. *Science of The Total Environment*, 622–623, 882–891.

<https://doi.org/10.1016/j.scitotenv.2017.11.327>

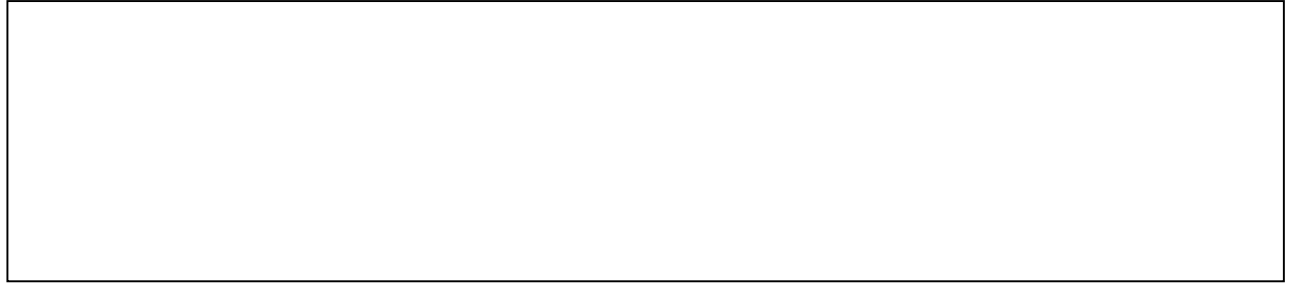
Zhang, W., Randall, M., Jensen, M. B., Brandt, M., Wang, Q., & Fensholt, R. (2021). Socio-economic and climatic changes lead to contrasting global urban vegetation trends. *Global Environmental Change*, 71, 102385. <https://doi.org/10.1016/j.gloenvcha.2021.102385>

Declaration of Interest Statement

The authors declare that they have no known competing financial interests or personal relationships that could have appeared to influence the work reported in this paper.

The author is an Editorial Board Member/Editor-in-Chief/Associate Editor/Guest Editor for this journal and was not involved in the editorial review or the decision to publish this article.

The authors declare the following financial interests/personal relationships which may be considered as potential competing interests:



Journal Pre-proof